

ENSO-coupled precipitation records (1959–2004) based on shells of freshwater bivalve mollusks (*Margaritifera falcata*) from British Columbia

Bernd R. Schöne · Nicholas A. Page ·
David L. Rodland · Jens Fiebig · Sven Baier ·
Samuli O. Helama · Wolfgang Oschmann

Received: 8 March 2006 / Accepted: 31 May 2006
© Springer-Verlag 2006

Abstract We present the results of sclerochronologically calibrated growth and stable isotope analyses of the freshwater bivalve *Margaritifera falcata* collected from an agricultural, suburban setting near Vancouver, BC. The oxygen isotope range of shell aragonite can be explained by the temperature range during the growing season, assuming the water $\delta^{18}\text{O}$ composition remained constant. However, shell growth is strongly influenced by local summer precipitation and potentially runoff of nutrient-rich stormwater. About 44% of the variability of annual shell growth can be explained by amounts of local summer (June–September) rainfall. Local winter precipitation and El Niño–Southern Oscillation (ENSO) strength during the preceding year exert a weak, but significant control on shell growth. In combination, summer and winter precipitation can explain up to 50% of the variability in annual shell growth. Spectral analyses substantiate the effect of precipitation on shell growth and demonstrate that shell growth and ENSO are coupled by precipitation. Common spectral density was found at periods of 6.5–9 years, particularly between 1985 and 2004. Higher frequency oscillation corresponding to periods of 3–5 years occurred during the early 1970s, early to mid 1980s,

and later 1990s. These results suggest that skeletal records of bivalve mollusks provide suitable archives of ENSO-coupled precipitation in areas where other climate proxies such as tree-rings and speleothems may not be available.

Keywords Sclerochronology · Stable isotope geochemistry · Runoff · Climate records · El Niño–Southern Oscillation

Introduction

Strong inter-annual and decadal-scale variations of precipitation can affect ecosystems and human societies. This is particularly true for rapidly growing populations in urban areas and agricultural landscapes such as the Lower Fraser Valley (LFV) region. Precipitation variability influences river discharge and the chemical composition of surface and groundwater. Increased precipitation can trigger unexpected floods that threaten housing, cause soil and stream channel erosion, and damage drainage infrastructure. Increased precipitation may also increase the transfer of contaminants from agricultural fields, urban areas, and industrial sites to sensitive aquatic ecosystems. In contrast, reduced precipitation may result in shortages of drinking water, reduce water available for irrigation, and affect fish populations through reduced stream flow.

It is well known that precipitation patterns across Canada and the contiguous United States are coupled to climate oscillations such as the Pacific Decadal Oscillation (PDO; 25–40-year cycles) and the El Niño–Southern Oscillation (ENSO; 2–7-year cycles) (Ropelewski and Halpert 1986, 1987, 1989; Groisman

B. R. Schöne (✉) · D. L. Rodland · J. Fiebig · S. Baier ·
S. O. Helama · W. Oschmann
INCREMENTS Research Group,
Institute for Geology and Paleontology,
University of Frankfurt, Senckenberganlage 32,
60325 Frankfurt/Main, Germany
e-mail: B.R.Schoene@em.uni-frankfurt.de

N. A. Page
Raincoast Applied Ecology, #102-1661 West 2nd Avenue,
Vancouver, BC, Canada V6J 1H3

and Easterling 1993; Ting and Wang 1997; Hsieh and Tang 2001; Jakob et al. 2003). Such large-scale analyses, however, cannot provide quantitative estimates of how the amount and timing of precipitation has changed at more regional scales over time. Knowledge of past variations of regional climate may be useful to predict the range, frequency, and intensity of future changes and estimate the effect of anthropogenic forcing of the regional hydrology. Such data may help decision makers in managing fish populations, drainage systems, water supply, and land use in sensitive watersheds, as well as understanding the broader physical processes that affect freshwater ecosystems.

In the LFV region of southwestern British Columbia, considerable effort has been spent on trying to describe, model, and understand the effects of urban and agricultural development on freshwater ecosystems (Wernick et al. 1998; Berka et al. 2001; Fluegel et al. 2004; Hall and Schreier 1996). However, limited resources for long-term monitoring have restricted the understanding of how freshwater ecosystems respond to longer-term climate variability. The lack of research on natural variability may have led to undue emphasis on the role of anthropogenic development as the driver of change in streams and rivers in the region. This viewpoint underlies approaches to assessing and monitoring discharge, water quality, and biota in the region.

Commonly used long-term, high-resolution proxy records for precipitation such as tree-rings (Stockton and Jacoby 1978; Meko et al. 1995; Gedalof et al. 2004) are not available for this largely deforested region. Here we present a new proxy record for summer precipitation in the Pacific Northwest which is coupled to superordinate climate forces (ENSO/PDO). Our new proxy is based on shells of the western pearlshell mussel, *Margaritifera falcata* (Gould), capable of extending observational records back in time.

Sample locality

Coghlan Creek is located in the Township of Langley in the LFV, British Columbia, Canada (Fig. 1). It is a tributary of the Salmon River which flows to the Fraser River near Fort Langley, BC. The Coghlan Creek watershed is approximately 13.8 km² with a total stream channel length of 19.5 km. Average flow-rate per second is 0.45 m³/s (Rood and Hamilton 1995). The stream channel is low-gradient (<2% slope) with sand and fine gravel substrate and extensive floodplain features such as flood benches and swamps. Fisheries values are high and Coghlan Creek supports healthy

populations of coho salmon, chum salmon, and cutthroat trout, as well as a variety of non-salmonid fishes (Fraser River Action Plan 1999; Giannico 2000).

Land cover in the LFV is dominated by agricultural and urban land uses (Boyle et al. 1997). Today, the LFV is Canada's third largest urban region and is home to about two million people. Approximately 52% of the Coghlan Creek watershed is used for agriculture while only 38% remains forested (GVS&DD 1999). The amount of impervious land cover, an indicator of urbanization, is 5%. The headwaters of Coghlan Creek are bisected by the Trans Canada Highway.

Water chemistry in Coghlan Creek is influenced by the intensity of urban and agricultural land use. Nitrate-N concentrations have been recorded as high as 7.1 mg/L during the summer when groundwater contributes a large portion of the stream flow (Wernick et al. 1998). Wernick et al. (1998) further suggested that these elevated nitrate-N concentrations in streamwater were caused by contamination of the shallow aquifer by septic systems and agricultural waste. Water temperature ranges from 12 to 17°C between June and September and from 3 and 8°C between November and March. During summer, the area receives only limited amounts of rain (Oke and Hay 1998) and agricultural crops require irrigation. Over 50% of this water is drawn from the Fraser River and its tributaries.

Materials and methods

Sixteen living and five dead specimens of *M. falcata* were collected between 22 September 2003 and 10 April 2005 from two adjacent localities from Coghlan Creek (NP1-... and NP2-...—49.121°N, 122.527°W; NP3-..., NP4-..., and NP5-...—49.127°N, 122.543°W; Fig. 1; Table 1). After removal of the soft parts from the life-collected material, all specimens were cleaned in de-ionized water and 99.5% EtOH and allowed to air-dry. Specimens were mounted on plexiglass cubes, and a protective layer of JB KWIK, a metal epoxy, was applied to the shell surfaces. We cut two ca. 2–3-mm thick cross-sections from each shell along the axis of minimum growth (Fig. 2a, b). All slabs were mounted on glass slides with the “mirroring” sides facing up and ground (800 and 1,200 grit SiC powder) on glass plates and polished (1 μm Al₂O₃ powder) on a Buehler G-cloth.

Correlation of growth and environmental records

Large-scale precipitation and temperature effects on the Coghlan Creek discharge were estimated from spatial

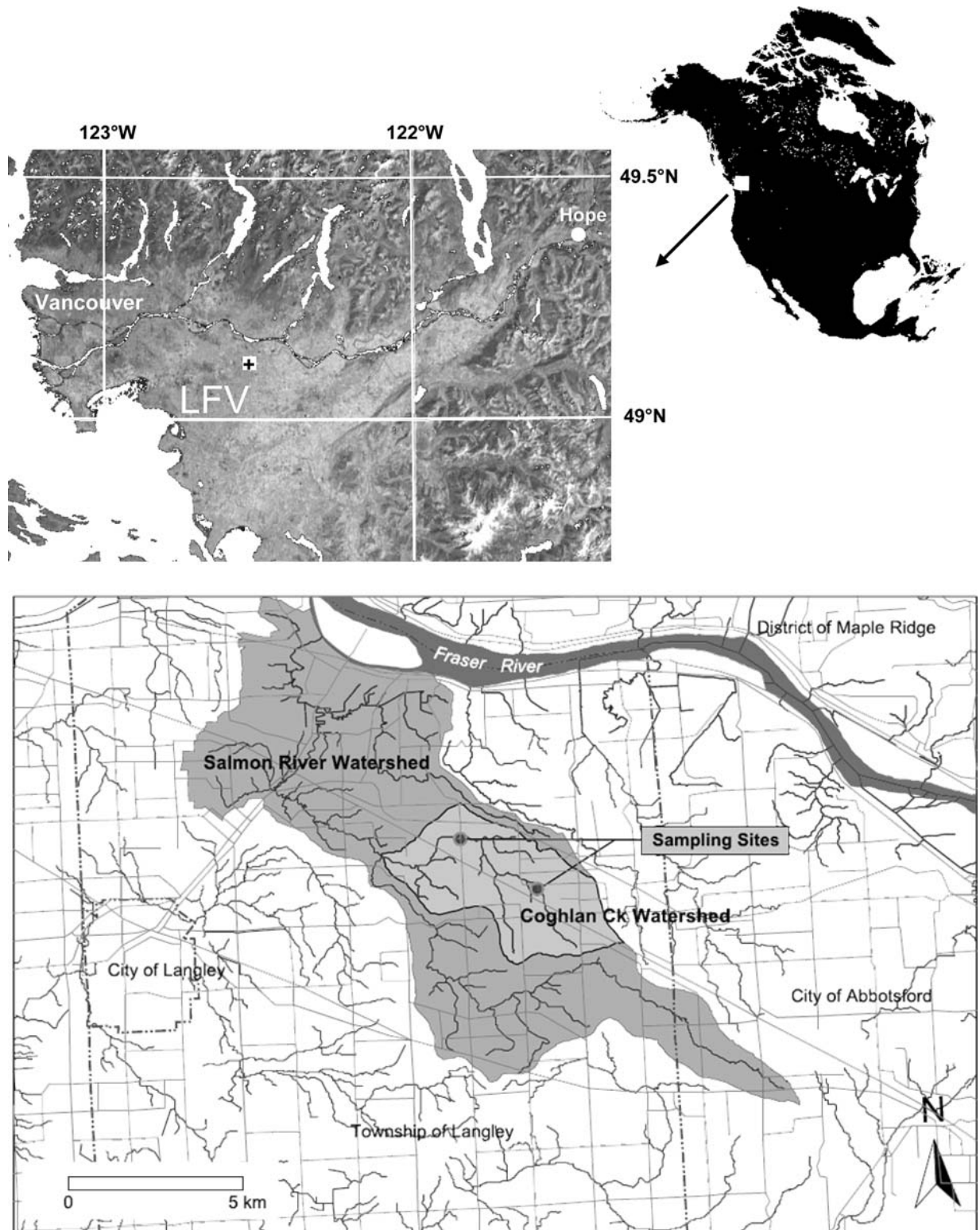


Fig. 1 Map showing sampling locality at Coghlan Creek (*cross*) in the LFV region. Map template taken from NASA WorldWind (<http://www.worldwind.arc.nasa.gov/>)

correlation (temperature and precipitation vs. shell growth, respectively) diagrams for each month using the KMNI Explorer (<http://www.climexp.knmi.nl>) and

HadCRUT2 temperature anomalies (Rayner et al. 2003) and Global Precipitation Climatology Centre (GPCC) precipitation data VASclimO (Variability

Table 1 List of specimens of *M. falcata* used in this study and purpose of use. “A” and “D” following dash in column “Specimen ID” stand for alive or dead collected, respectively

Specimen ID	Purpose		# $\delta^{18}\text{O}$ samples	Ontogenetic age (yr)	# measurable annual increments	Date of collection	Year of death
	SGI	$\delta^{18}\text{O}$					
NP1-A1R	X			29	25	27 Sep 2004	2004
NP1-A2R	X			31	25		
NP1-A3L	X			29	24		
NP1-A5L	X	X	25	22	17		
NP1-A6R	X			16	11		
NP2-A1L	X			33	29		
NP2-A2L	X			22	18		
NP2-A3L	X			21	16		
NP2-A4L	X			16	13		
NP2-A5L	X			16	13		
NP2-A6L		X	31	10			
NP4-A1L	X	X	59	39	33	10 Apr 2005	2005
NP4-A2L	X			31	25		
NP4-A4L	X			29	22		
NP4-A5L	X			36	30		
NP4-A6L	X			52	46		
NP5-D1L	X			28	25		
NP5-D2L	X			10	7		2000
NP3-D1R	X			34	31		1992
NP3-D2R	X			28	21		2000
NP3-D4R	X			28	21		1983

Analysis of Surface Climate Observations; joint project between the German Weather Service and the University of Frankfurt, Institute for Atmosphere and Environment, Climatology Department; <http://www.dwd.de>). Furthermore, shell growth was compared to the NINO1.2 (0–10°S, 80–90°W) and NINO3 (5°N–5°S, 90–150°W) indices (<http://www.cdc.noaa.gov/ClimateIndices>). For establishing a growth-precipitation model, multiple linear regression analyses were conducted for annual shell growth and monthly precipitation rates close to the sample locality (data obtained from the NOAA Climate Diagnostics Center, <http://www.cdc.noaa.gov>).

Sclerochronology

To resolve shell-internal microgrowth patterns, one polished cross-section from each specimen was immersed in Mutvei’s solution for 23 min at 37–40°C with constant stirring. Mutvei’s solution (Schöne et al. 2005) consists of 0.5% acetic acid, 12.5% glutaraldehyde and ca. 10 g of alcian blue per liter solution. This agent simultaneously etches the carbonate, preserves the organic framework and stains mucopolysaccharides, thereby increasing the visibility of the microgrowth structures. Immediately after immersion, the samples were carefully rinsed in de-ionized water and air-dried.

Etched sections were viewed under a reflected light binocular microscope at magnifications of 20–75× and

digitized with a Nikon Coolpix 995 camera (Fig. 2c, d). The custom-designed image analysis software Panopea[®] was used for measuring the widths of annual increments (m_t) in the outer shell layer.

In order to isolate environmental signals from increment width time-series, ontogenetic trends must be removed (Cook and Kairiukstis 1990). As the mussel grows older, the rate of shell accretion decreases. Age-related trends were estimated with stiff cubic splines (p_t) that retained all high-frequency oscillations and most of the low-frequency, i.e., quasi-decadal oscillations. Age-trends were eliminated from the increment time-series by dividing measured by predicted growth:

$$\text{GI} = \frac{m_t}{p_t} \quad (1)$$

Standardization transformed the stationary growth index (GI) values into standardized growth indices (SGI; Jones et al. 1989):

$$\text{SGI} = \frac{\text{GI} - \bar{x}_{\text{GI}}}{\sigma_{\text{GI}}}, \quad (2)$$

where \bar{x} is the average and σ the standard deviation of all GI values of a time-series. SGI values are dimensionless measures of shell growth and enable direct comparison of shell growth of different specimens or of different ontogenetic stages of growth within one.

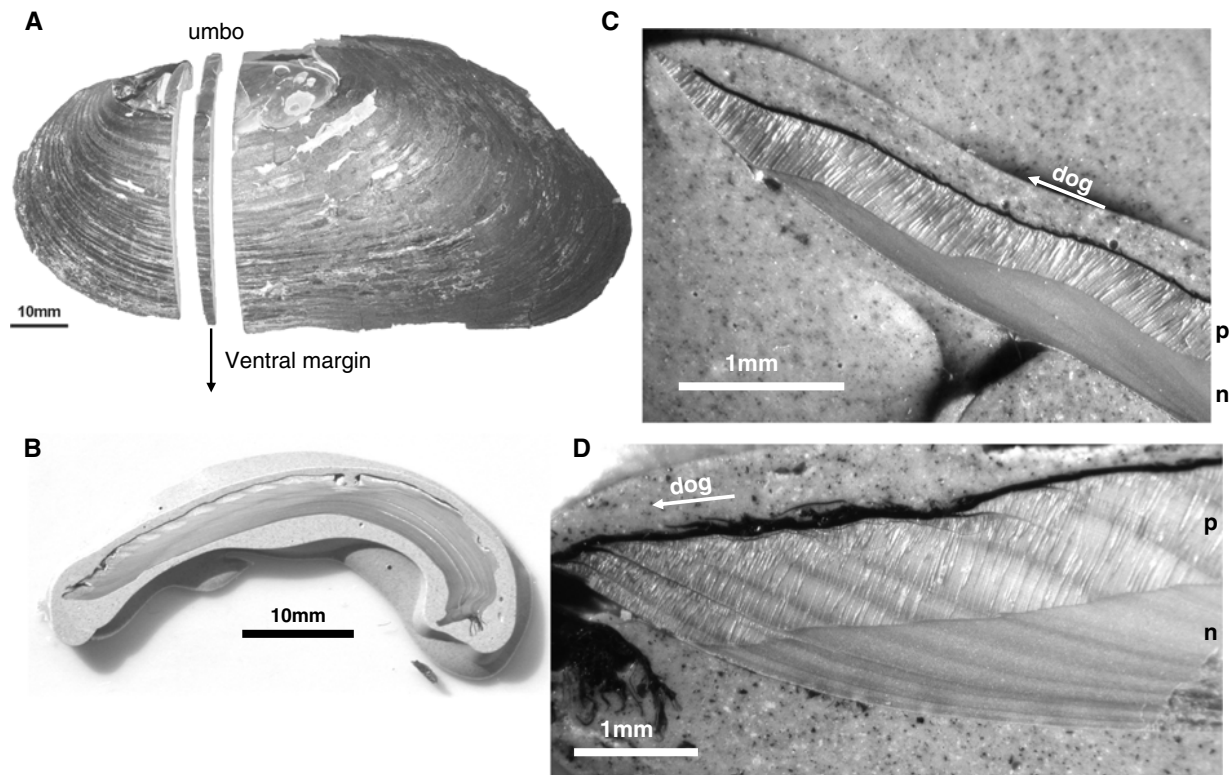


Fig. 2 For analysis of internal growth structures, shells of *M. falcata* were cut along the axis of minimum growth and perpendicular to the growth lines (**a**). A 2-mm thick slab was mounted on a glass slide, ground, polished, and immersed in Mutvei's solution (**b**). This treatment revealed annual growth structures consisting of annual growth increments separated by distinct growth lines (**c**, **d**). Note that microgrowth increments

are broader in *light-colored shell portions* half-way through annual increments than in *dark shell portions* near annual growth lines. **c** At the ventral margin of specimen NP2-A7R, collected alive on 22 September 2003, an annual growth line is about to form. **d** A new annual increment has already started to form in specimen NP4-A4L, which was live-collected on 10 April 2005. *p* prismatic, *n* nacreous shell layer, *dog* direction of growth

Individual SGI time-series were combined in a single master chronology by calculating the arithmetic mean of the SGI values at each year. As a measure of the robustness of the master chronology, we computed the expressed population signal (EPS; Wigley et al. 1984; Briffa and Jones 1990):

$$\text{EPS} = \frac{nR_{\text{av}}}{nR_{\text{av}} + (1 - R_{\text{av}})}, \quad (3)$$

where n is the number of specimens and R_{av} the inter-series correlation (average of all correlation coefficients). The EPS value quantifies the similarity between the averaged chronology and the theoretical infinitely replicated chronology for the appropriate inter-series correlation (Wigley et al. 1984; Briffa and Jones 1990). EPS values greater than 0.85 are considered statistically significant (Wigley et al. 1984; Cook et al. 2000).

Spectral analyses

For spectral analyses, linear growth trends were removed from both the master chronology and

instrumental data, and continuous wavelet transforms were computed (CWT; zero-padding to adjust for edge effects, Morlet wavelet, wavenumber: 8). CWTs reveal inherent frequencies of time-series data and determine their strength and evolution through time.

Stable isotope geochemistry

The remaining cross-sectioned slabs were used for stable oxygen and carbon isotope analyses. Prior to sampling, epoxy resin, periostracum and secondary shell layers were mechanically removed. Following the shape of the microgrowth increments, aragonite powder was milled from the outer shell layer of the bivalves. For this purpose we used a cylindrical diamond-coated drill bit (1 mm diameter). A total of 115 individual millings were completed (Fig. 3). Each milling step perpendicular to the direction of growth measured approximately 100 μm and yielded about 60 μg of carbonate powder, and corresponded to a temporal resolution of about 10–18 days per sample. Samples were processed in a Finnigan MAT 253

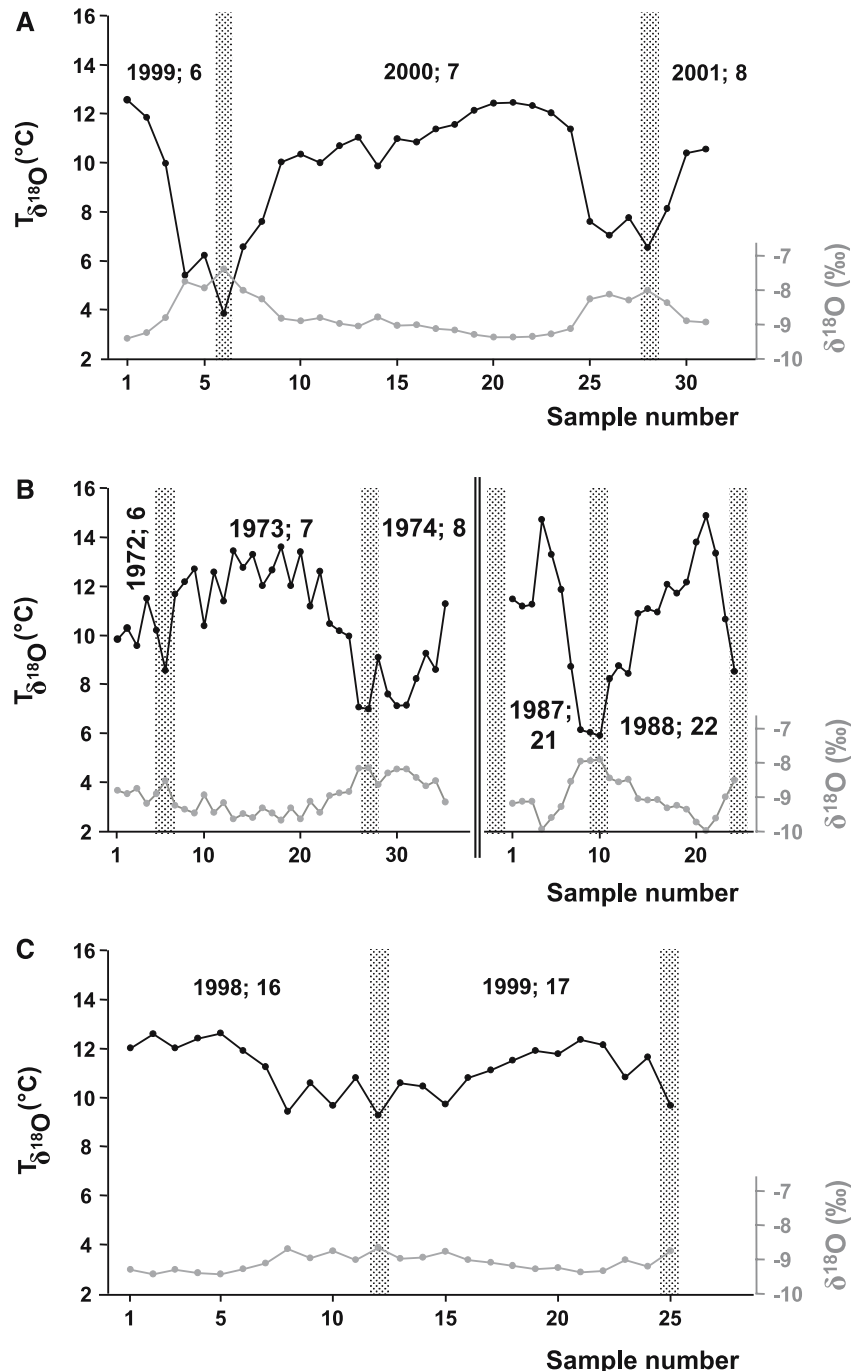
continuous-flow mass spectrometer equipped with a Gas Bench II. Shell isotope values are reported relative to VPDB based on a NBS-19 value of -2.20‰ for $\delta^{18}\text{O}$ and 1.95‰ for $\delta^{13}\text{C}$. On average, replicated precision (multiple measurements of the NBS standard) was better than 0.07‰ (1SD) for $\delta^{18}\text{O}$ and better than 0.05‰ (1SD) for $\delta^{13}\text{C}$.

Oxygen isotope ratios of calcium carbonate can be used to reconstruct water temperatures ($T_{\delta^{18}\text{O}}$).

We used the paleothermometry equation of Grossman and Ku (1986). A small modification of their equation was required because they report water values in VSMOW— 0.2‰ (Goodwin et al. 2001). The corrected function is as follows:

$$T_{\delta^{18}\text{O}(\text{aragonite})}(\text{°C}) = 20.60 - 4.34 \times (\delta^{18}\text{O}_{\text{aragonite}} - (\delta^{18}\text{O}_{\text{water}} - 0.20)).$$

Fig. 3 Shell oxygen isotopes between successive major growth lines (vertical bars) reveal annual temperature cycles. Temperature reconstructions are based on the paleothermometry equation of Grossman and Ku (1986) assuming $\delta^{18}\text{O}_{\text{water}}$ values of $-11.08 \pm 0.36\text{‰}$ (mean \pm 1SD; adapted from Wassenaar 1995). Error in temperature reconstructions (1SD) is thus 1.6°C . Note that water temperatures reconstructed from shell oxygen isotopes of specimens NP2-A6L (a) and NP4-A1L (b) are close to ambient water temperatures that prevail during the growing season ($3.8\text{--}12.37$ and $6\text{--}15\text{°C}$, respectively). However, the actual temperature range during the growing season was underestimated by specimen NP1-A5L (c; 3.1°C) suggesting large seasonal fluctuations of the $\delta^{18}\text{O}_{\text{water}}$ values. Numbers separated by semicolon stand for year AD and ontogenetic age



Results

Etched cross-sections of *M. falcata* shells exhibit an alternating pattern of distinct annual (Chamberlain 1931; Bauer 1992; Metcalfe-Smith and Green 1992; Johnson and Brown 1998) growth increments and growth lines (Fig. 2c, d). Broadest annual increments measured 4 mm (NP2-A2L; age 4) and narrowest 15 μm (NP4-A3L; age 39). In the direction of growth, the light-colored (prismatic) to light-blue (nacreous shell layer) treated growth increments become successively darker brown toward the following increment. A sharp line separates two adjacent annual increments. At higher magnification (75 \times), micrometer-scale increments and lines (microgrowth patterns) can be discerned within the annual growth increments (Fig. 2c, d). Narrowest microgrowth increments (<1 μm) were observed in the brown portions of the annual increments. In specimens collected during late September, the brown zone was present near the ventral margin (most recently formed shell portion), but a distinct annual growth line had not yet formed (Fig. 2c). Specimens from early April, however, showed a distinct growth line near the commissure and about one-tenth of a new annual increment (Fig. 2d).

Based on increment counts in the prismatic and nacreous layers, we determined the ontogenetic age of the shells. The oldest specimen was at least 46 years old, the youngest had attained age 7 (Table 1). Corrosion of umbonal shell portions precluded an exact age determination in shells older than 10–15 years.

Oxygen isotope measurements

Shell $\delta^{18}\text{O}$ profiles determined between successive growth lines revealed clear annual cycles. Most positive values of -7.4 to -8.67‰ were found near the growth lines, while most negative values occurred approximately half-way between two annual growth lines (-9.38 to -9.97‰ ; Fig. 3). Minimum and maximum intra-annual $\delta^{18}\text{O}_{\text{aragonite}}$ ranges were 0.71% (Fig. 3c—specimen NP1-A5L, year 1999, age 17) and 2.03% (Fig. 3b—specimen NP4-A1L, year 1987, age 21), respectively.

Ensembles of growth increment time-series

Age-detrended and standardized growth increment time-series of live-collected specimens compared well to each other, exhibiting a high running similarity (Fig. 4a). The good visual agreement between the individual SGI time-series was substantiated by an

EPS value of 0.87. We combined the SGI curves of 15 specimens (Table 1) collected alive into a single master chronology that covers the time interval of 1959–2004 (Fig. 4b). Ninety-five percent confidence intervals of the master chronology (Fig. 4c) are narrower for more recent times, i.e., for larger sample sizes (Fig. 4d).

Aside from the typical corrosion near the umbo of ontogenetically older shells, dead collected shells were perfectly preserved. Their commissural lines were intact, with their valves still articulated at the hinge, the periostracum present and the degree of corrosion similar to living shells. It was possible to integrate the SGI curves of the dead collected shells into the master chronology by visual cross-dating. As a result, the EPS value improved slightly to 0.88. According to cross-dating, the dead collected shells died within the last 22 years (Table 1).

Master chronologies, temperature, precipitation, and El Niño

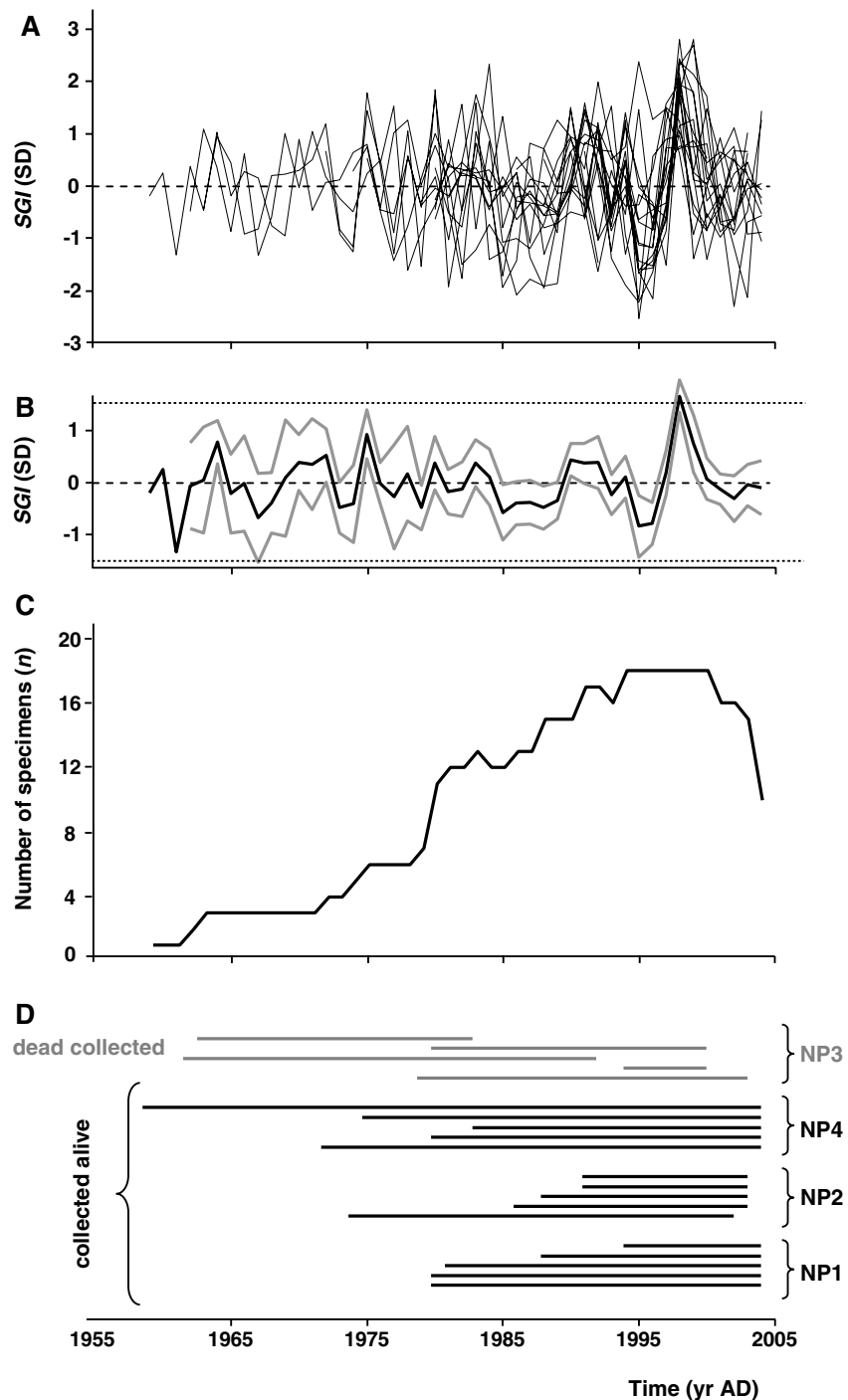
Spatial correlation charts indicate a good agreement between shell growth and precipitation during June through August, but only a weak to non-existent correlation between shell growth and temperature (predictor variables; Fig. 5a, b). A weak positive correlation ($R < 0.3$) was found between shell growth and November and December of the previous year, and a weak negative ($R < -0.4$) correlation between growth and June of the current year (Fig. 5a). For precipitation and shell growth, R values range between 0.4 and 0.6 (Fig. 5b). A weak correlation (R values of 0.2–0.3) also exists between the master chronology and precipitation during January (Fig. 5b). Interestingly, highest correlation coefficients were found between shell growth and precipitation in the mountains south and northeast of the LFV (Fig. 5b).

Multiple linear regression models were computed (stepwise forward modeling) to further evaluate the effect of variable precipitation rates on shell growth. Within SGI values of $+1.5\text{SD}$ and -1.5SD (this excludes the strong El Niño year of 1997/1998) between 44 and 50% of the variation in annual shell growth can be explained by precipitation close to the sample locality (Fig. 5b). In the first model (Eq. 4), precipitation during summer and winter (January, June through September; JJJAS; $R = 0.71$, $R^2 = 0.50$) was included:

$$\text{SGI} = 0.004 \times P_{\text{Jan}} + 0.015 \times P_{\text{Jun}} + 0.003 \times P_{\text{Jul}} + 0.011 \times P_{\text{Aug}} + 0.004 \times P_{\text{Sep}} - 1.087. \quad (4)$$

Fig. 4 Annual increment width time-series of *M. falcata*. *SD* indicates standard deviation units.

a Standardized annual growth increment (SGI) time-series of all 20 specimens. Note high degree of running similarity between the individual chronologies. **b** Master chronology constructed from the 20 specimens shown in (a) (black line arithmetic mean, gray lines 95% confidence intervals). The SGI master chronology stretches over the period of AD 1959–2004. **c** Sample sizes—number of specimens used per year. **d** Time span covered by the specimens. Each line stands for one individual specimen of *M. falcata*



Based on the coefficients for precipitation of each month given (Eq. 4), a new time-series for winter and summer precipitation (P_{JJAS}) was computed:

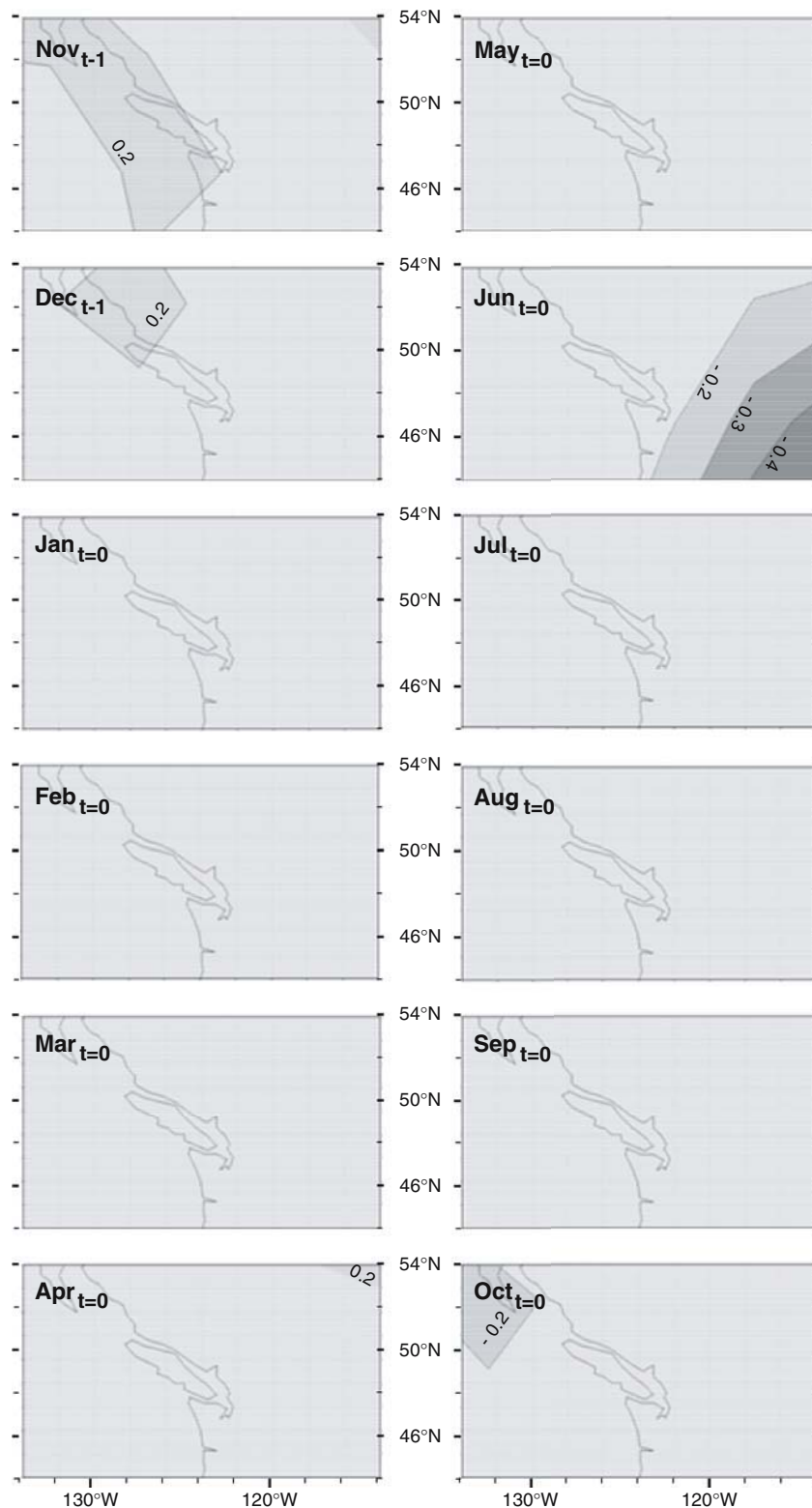
$$P_{JJAS} = 13.65 \times \text{SGI} + 29.06. \quad (5)$$

Equation 5 ($R = 0.71$, $R^2 = 0.50$, $p < 0.0001$; Fig. 6a, b) can be used to reconstruct average precipitation during January plus June through August. Precipitation during

January alone explains 11% ($R = 0.33$, $R^2 = 0.11$, $p < 0.04$).

In a second multiple linear regression model (Eq. 6), we only included precipitation rates during the warm season (June through September, JJAS; within SGI limits of $-1.5SD$ and $1.5SD$). Shell growth and precipitation rates of June through September were positively correlated ($R = 0.66$, $R^2 = 0.44$).

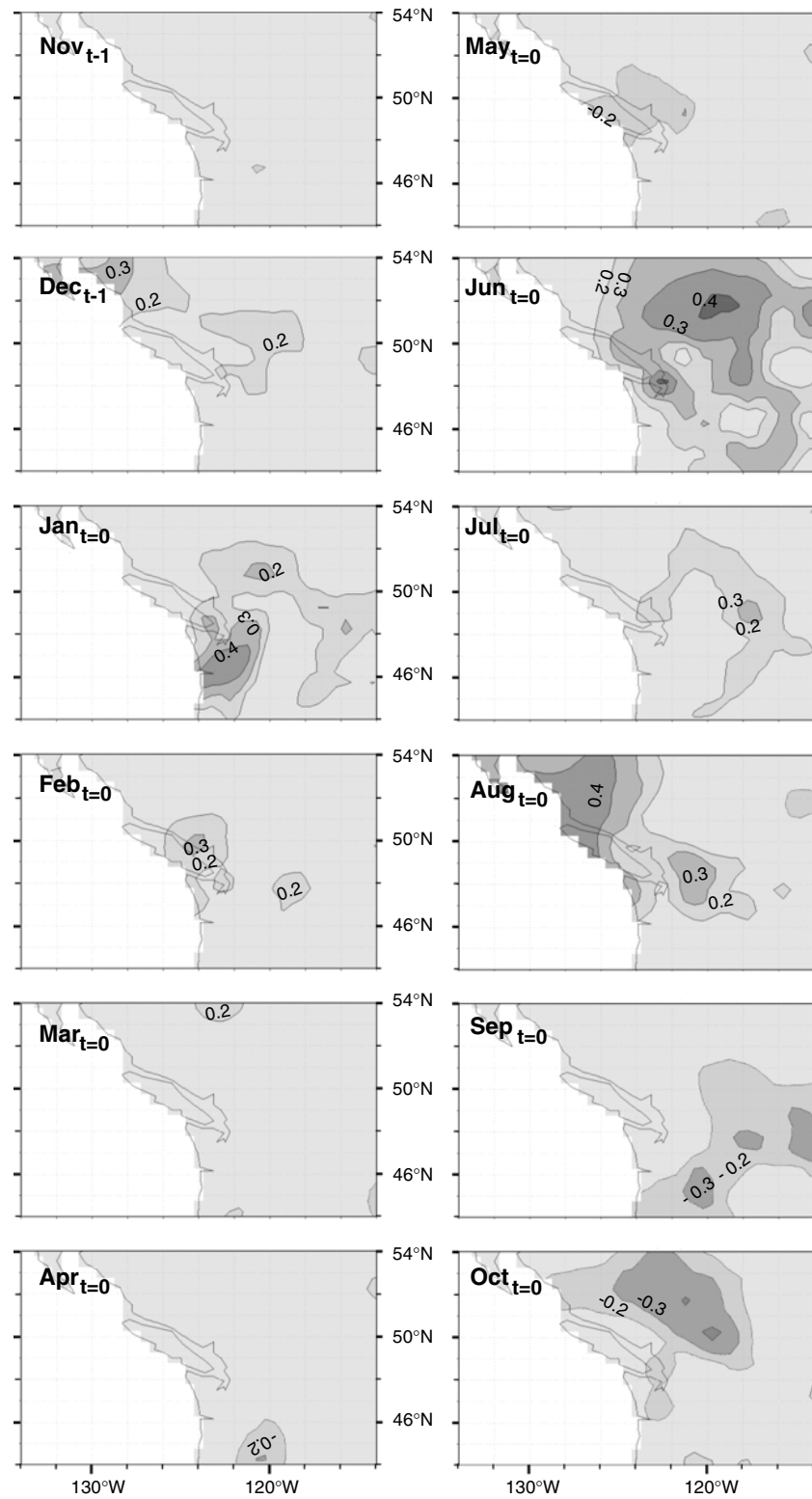
Fig. 5 a Monthly spatial correlation charts between shell growth and gridded temperature (HadCRUT2 temperature anomalies) from November of the previous year ($t-1$) to October of the current year (t). Shell growth and temperature exhibit very little to no correlation.
b Monthly spatial correlation charts between shell growth and gridded precipitation from November of the previous year to October of the current year (VASclimO, 1951–2000 GPC analysis). Shell growth is strongly positively correlated with summer precipitation and weakly with winter precipitation. Diagrams were created with the KMNI explorer (<http://www.climexp.knmi.nl>). Lightest gray coverage of meteorological data, gray map contours with numbers = R values (correlation coefficients). Note that each contour color comprises an R value range of 0.1 starting with the lowest R value, e.g., “0.2” stands for 0.2–0.29 and “-0.3” stands for -0.3 to -0.39



$$\begin{aligned}
 \text{SGI} = & 0.016 \times P_{\text{Jun}} + 0.004 \times P_{\text{Jul}} \\
 & + 0.011 \times P_{\text{Aug}} + 0.005 \times P_{\text{Sep}} - 0.952. \quad (6)
 \end{aligned}$$

Based on the coefficients for precipitation of each month given (Eq. 6), a new time-series for summer precipitation (P_{JJAS}) was computed:

Fig. 5 continued



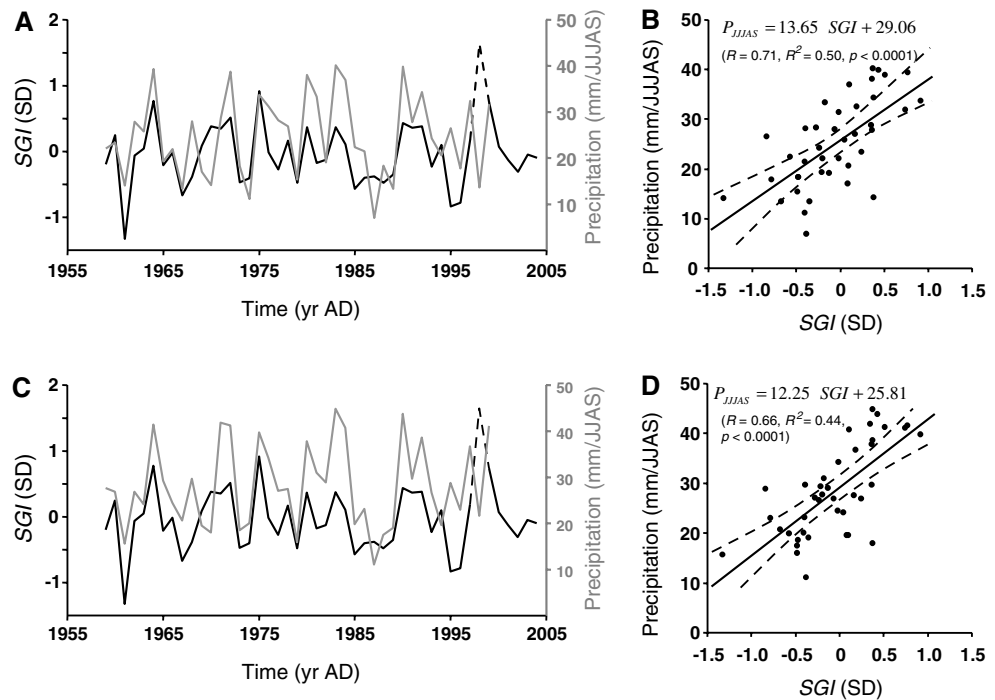
$$P_{JJAS} = 12.25 \times SGI + 25.81. \quad (7)$$

Equation 7 ($R = 0.66, R^2 = 0.44, p < 0.0001$; Fig. 6c, d) can be used to reconstruct summer precipitation rates

(mm per month) from annual increment widths of *M. falcata*.

Shell growth also co-varied significantly (95% confidence level) with the NINO1.2 and NINO3 indices of

Fig. 6 Relative annual shell growth (SGI) and precipitation. **a** Relative annual shell growth compares well to precipitation during January plus June through September (P_{JJAS}). **b** The linear model can be used to reconstruct mean P_{JJAS} from SGI. **c** Relative annual shell growth compares well to precipitation during the time interval between June and September (P_{JJAS}). **d** The linear model can be used to reconstruct mean P_{JJAS} from SGI. About 44% of the variability in SGI is explained by P_{JJAS} . Dashed lines 95% confidence intervals of the line fits



the preceding year. Highest explained variability was found for SGI values and the NINO1.2 index of August of the previous year ($NINO1.2_{Aug(t-1)}-R = 0.40, R^2 = 0.16, p = 0.01$). A correlation matrix is given in Table 2.

Spectral analysis

Continuous wavelet transformations of the SGI, P_{JJAS} , P_{JJAS} , and $NINO1.2_{Aug(t-1)}$ index time-series compared well to each other (Fig. 7). Coherent spectral power was found at frequencies corresponding to periods 6.5 and 9 years, most prominently between 1985 and 2004. Weaker common spectral power was also present at periods of about 3–5 years during the early 1970s and late 1990s. Precipitation records,

however, did not reveal spectral power at these higher frequencies after the mid 1980s (Fig. 7b, c).

Discussion

As in a variety of other margaritiferid species (Bauer 1992; Schöne et al. 2004), major growth lines and increments of *M. falcata* from Coghlan Creek form on an annual basis. Based on collections at different seasons of the year, the growing period can be narrowed down to March/April through October. A similar growth period has been observed in *M. falcata* in two populations approximately 200 km to the south (Toy 1998). During these months, air temperature usually exceeds 5°C, which is approximately the lower

Table 2 Correlation matrix of shell growth vs. NINO1.2 and NINO3 index, respectively

Month	SGI-NINO1.2 (n = 46)			SGI-NINO3 (n = 46)		
	R	R ²	p	R	R ²	p
May _{t-1}	0.33	0.11	0.03	0.29	0.08	0.05
Jun _{t-1}	0.33	0.11	0.03	0.27	0.07	0.07
Jul _{t-1}	0.35	0.12	0.02	0.30	0.09	0.04
Aug _{t-1}	0.40	0.16	0.01	0.31	0.10	0.04
Sep _{t-1}	0.37	0.14	0.01	0.30	0.09	0.04
Oct _{t-1}	0.35	0.13	0.02	0.30	0.09	0.04
Nov _{t-1}	0.32	0.11	0.03	0.29	0.08	0.05
Dec _{t-1}	0.26	0.07	0.01	0.26	0.07	0.08
Jan _{t = 0}	0.27	0.07	0.07	0.31	0.10	0.04

t-1 indicates previous year, t = 0 is current year

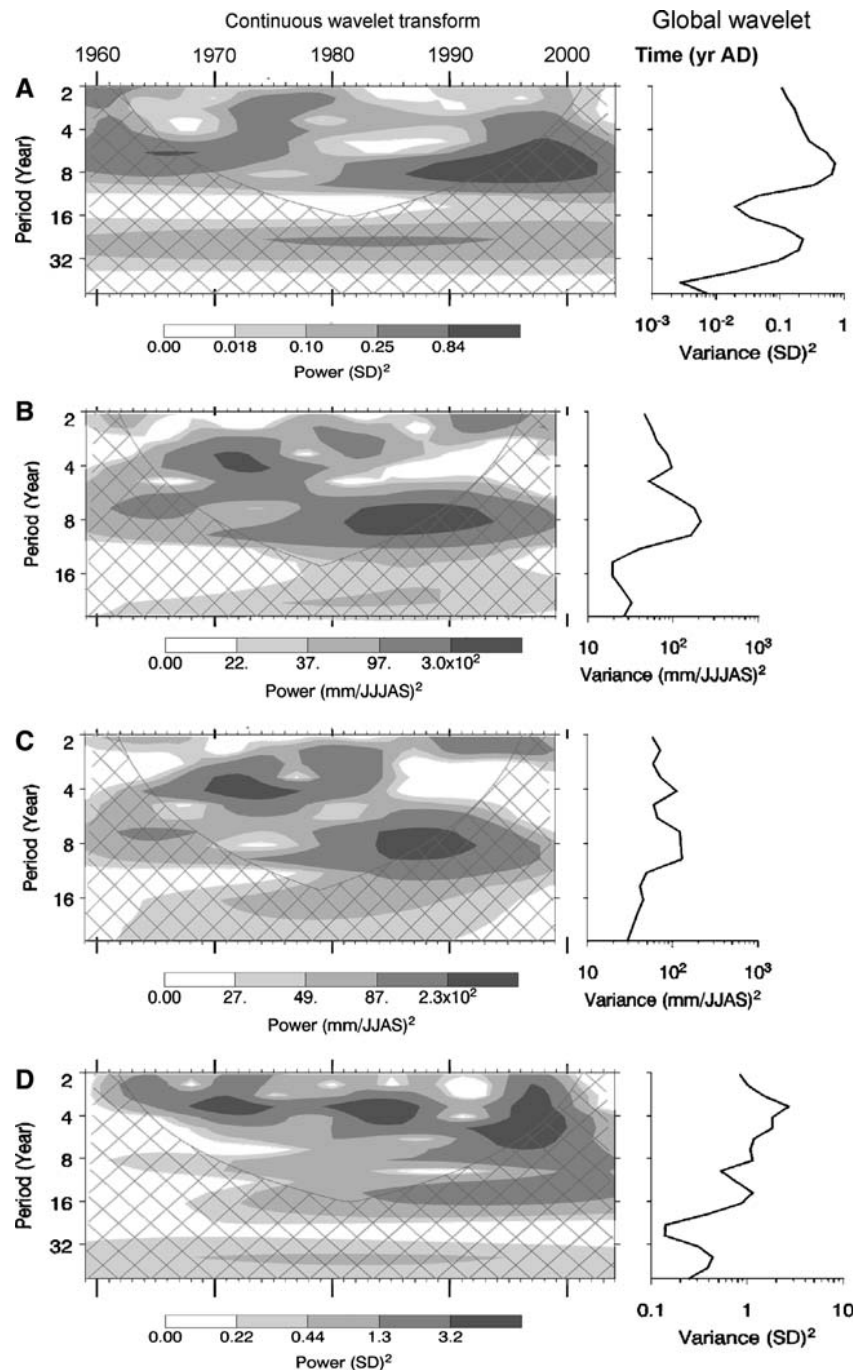


Fig. 7 Continuous wavelet spectra and global wavelets (ION script at <http://www.ion.researchsystems.com>; after Torrence and Compo 1998) of age-detrended SGI curves (a), precipitation during January plus June through September (P_{JJJAS} ; b), precipitation during summer (P_{JJAS} ; c) and NINO1.2_{Aug(t-1)} index (d). Wavelet transforms reveal distinct common spectral power at approximately 6.5–9 years, particularly during the time

growth temperature threshold for *Margaritifera margaritifera* (Dunca and Mutvei 2001). It seems likely that the timing of the growing period is controlled by similar shutdown temperatures in different species of the genus *Margaritifera*.

interval 1985–2004. During the early 1970s, early to mid 1980s, and late 1990s, weaker spectral density was observed at periods of about 3–5 years in almost all records. The contour levels are chosen so that 75, 50, 25, and 5% of the wavelet power is above each level, respectively. The *cross-hatched region* refers to the cone of influence, where zero padding has reduced the variance

Effect of temperature and precipitation on shell growth

The high running similarity between individual SGI time-series and EPS values in excess of 0.85 (threshold

value defined by Cook et al. 2000) suggest that shell growth of all specimens from Coghlan Creek was governed by similar, external forcings. Numerous studies on bivalve mollusks have identified temperature, pollutants, and food as major controls of shell growth (Ansell 1968; Kennish et al. 1994; Goodwin et al. 2001; Schöne et al. 2003; Dunca et al. 2005). In unpolluted streams with constant nutrient supply throughout the growing season, temperature exerts the dominant influence on shell growth of freshwater bivalves. This was observed for pristine, densely forested regions in Sweden where runoff of nutrients from soils into the river is limited (Schöne et al. 2004; Dunca et al. 2005).

In streams with anthropogenically altered water chemistry and quality, however, temperature often plays a subordinate role in controlling shell growth (see Fig. 5a). Increased acidity or sublethal concentrations of metals, polycyclic aromatic hydrocarbons, and chlorophenolics can impair biotic growth (McLeay 1987; Culp and Lowell 1999) and result in strongly diminished growth rates of freshwater bivalves (Dunca et al. 2005). In fact, freshwater bivalves are considered as ideal bioindicators of aquatic health because of their responsiveness to environmental disturbance (Mutvei and Westermark 2001). However, not all contaminants are deleterious to the riverine biota (McLeay 1987). High levels of phosphorus and nitrogen promote algal growth (eutrophication) and general productivity in the river (McLeay 1987; Hansson 1987; Feder and Pearson 1988; Hall et al. 1991). An extreme increase in annual shell growth was observed in *M. margaritifera* in years subsequent to an extended eutrophication of the Kvarnbäcken River in central Sweden (Dunca et al. 2005).

Here, we found a strong positive correlation between shell growth and summer precipitation ($R^2 = 0.44$). We interpret this finding as the result of increased food concentrations in the streamflow, primarily caused by surface water runoff of organic particles and nutrients from the surrounding fields during increased precipitation. Similar observations were recently made for margaritifera and unionid bivalves from uncontaminated rivers in northern Sweden. Concurrent with deforestation near the Nuortejaurbäcken River in the mid 1980s, shell growth rates increased significantly as the result of increased contents of organic particles in surface water runoff (personal communication, E. Dunca 2006).

Shell growth appears to be influenced by increased runoff of nutrient-rich water from agricultural and urban lands, and the increased contribution of nitrate-N contaminated groundwater flow to Coghlan Creek during the summer months. Surface runoff picks up

organic particles from exposed soils and rapidly conveys them to the stream channel through ditches and stormwater pipes in developed portions of the watershed. In addition to naturally occurring nutrients, a broad array of trace metals and organic contaminants including fertilizers, pesticides, and manure applied to agricultural land are conveyed to the stream through surface runoff or shallow groundwater. A number of studies have measured the concentrations of pollutants in streams and rivers of the LFV—a region renowned for its extensive agricultural activity, high livestock density, and increasing urbanization (Schreier et al. 1999; Wassenaar 1995; Hall and Anderson 1988; Macdonald et al. 1997; Fluegel et al. 2004). The effect of nutrient-rich runoff on shell growth is increased because agricultural activity is most intensive during the summer, which corresponds to the growing season of freshwater mussels. At the same time, streamflows are reduced and contaminants carried into the stream are less dilute. While the diffuse nature of these non-point sources of pollution makes them hard to quantify, nitrate levels are significantly higher in Coghlan Creek during summer than in winter (Wernick et al. 1998; Schreier et al. 1999). These results suggest that the impact of increased nutrient flux on shell growth is greater than the deleterious effects of trace metals and other pollutants, at least in the catchment area studied here.

ENSO and shell growth

A weak but significant positive correlation also exists between shell growth and winter precipitation rates (P_{Jan} — $R^2 = 0.11$, $p = 0.04$) and sea surface temperature anomalies in the Pacific during the preceding summer and fall akin to the ENSO (NINO1.2 $_{Aug(t-1)}$ — $R^2 = 0.16$, $p = 0.01$). This was further supported by common spectral power in wavelet transform of these time-series. The length of the time-series was not sufficient to evaluate the role of longer period signals such as the PDO. Since the pioneering studies by Walker (1923), it is well known that global and regional winter precipitation patterns are associated with the Southern Oscillation, the atmospheric component of ENSO. Shabbar et al. (1997) demonstrated that precipitation rates of British Columbia are significantly influenced by the Southern Oscillation phenomenon. In this region, strong El Niño events (warm periods) are followed by dry winters, while positive precipitation anomalies occur in years after La Niña events (Edmonds et al. 2003). During El Niño events, the warming of the air over the eastern tropical Pacific energizes the polar jet stream. As a

consequence, a strong low-pressure system develops over the Aleutians, pumping abnormally warm, dry air into western Canada, Alaska and the northern United States (Molnar and Cane 2002). The link between shell growth and ENSO is also reflected in common spectral power, particularly, at periods of 2–7 years, i.e., the typical ENSO-type oscillations (Trenberth 1997; Cane 2005). Note that the NINO1.2 and NINO3 indices to which shell growth was compared are ideal measures of the oceanic aspects of ENSO that influence the extratropical climate (Hoerling and Kumar 1977).

Shell oxygen isotopes: implication for water temperature and hydrology

Bivalve mollusks are considered to form their shells in oxygen isotopic equilibrium with the ambient water (Epstein et al. 1953; Mook and Vogel 1968; Wefer and Berger 1991). Isotope ratios of shell carbonate can hence be used to reconstruct environmental conditions such as water temperature or to identify water sources (Weidman et al. 1994; Bice et al. 1996; Marsh et al. 1999). Oxygen isotope values of *M. falcata* shells in Coghlan Creek showed distinct annual cycles that may partly reflect the temperature variability during the growing season, further substantiating the annual formation of shell carbonate. If the oxygen isotope composition of the river water remained constant throughout the growing season, the maximum observed seasonal $\delta^{18}\text{O}_{\text{aragonite}}$ range of 2.03‰ (Fig. 3b—specimen NP4-A1L, year 1987, age 21) would translate into a temperature range of 8.8°C. This almost perfectly matches the temperature range of the water during the March/April through October growing season, i.e., 9.7°C (Fig. 3).

Estimation of absolute water temperature from the above-mentioned $\delta^{18}\text{O}_{\text{aragonite}}$ values requires knowledge of the isotopic composition of the water in which the shells lived. Direct measurements of the isotopic composition of the Coghlan Creek aquifer or river are not available. A nearby aquifer (Abbotsford) located at the same height above sea level, however, exhibits an average $\delta^{18}\text{O}$ composition of approximately $-11.08 \pm 0.36\text{‰}$ (mean \pm 1SD; Wassenaar 1995). Using this value, the modified paleothermometry equation (Grossman and Ku 1986; Goodwin et al. 2001) returns temperatures of 3.8 and 15°C for the most extreme $\delta^{18}\text{O}_{\text{aragonite}}$ values of -7.4‰ (Fig. 3a; 1999) and -9.97‰ (Fig. 3b; 1987), respectively. 1SD error in temperature estimates is 1.6°C. The minimum and maximum measured temperatures during the growing season were 4.1°C in 1999 and 14.9°C in 1987, respectively. Hence, reconstructed and measured

temperatures compare extremely well to each other. This result demonstrates that shells of *M. falcata* actually form their valves in oxygen isotopic equilibrium with the ambient water.

The oxygen isotopic composition of the aquifer (-11.08) closely resembles the isotopic composition of the local precipitation: -10‰ (annual mean adjusted for variable amounts of precipitation; IAEA 2001). This value is based on monthly data from the station “Victoria” (N48.65°, W123.43°) determined over 30 years of observation. Note that maximum rainfall in the LFV occurs during winter when oxygen isotope values of the precipitated water are 2‰ more negative than the annual mean, i.e., -12‰ . It seems likely that aquifers of the LFV are mainly recharged during the winter period and their isotopic compositions are buffered by winter precipitation. In contrast, the water of the Fraser River is about 7–8‰ more negative than precipitation (-17.04‰ in July 1993, -17.85‰ in November 1993; measured at Alexandra Bridge near Hope; Cameron et al. 1995). Recharge of the aquifers from the Fraser or runoff from adjacent mountains to the south is probably only minor. We hence conclude that local precipitation is the main source for recharging the Coghlan Creek aquifer.

It should be noticed that the minimum observed $\delta^{18}\text{O}_{\text{aragonite}}$ range within the bounds of two consecutive annual growth lines (Fig. 3c—specimen NP1-A5L, year 1999, age 17) was 0.71‰, implying a temperature range of only 3.1°C, far less than the true temperature range. It seems unlikely that the growing season had been shortened dramatically: we exclusively sampled shell material from ontogenetically young (vigorously grown) specimens and, in addition, the same sampling resolution was applied to all shells. A more likely explanation for the observed differences in the temperature ranges among annual growth increments of different specimens is inter-annual and seasonal change in the isotopic composition of the water in which the shells lived. Possible controls of the isotopic composition may include irrigation of adjacent fields (Fraser River Action Plan 1999) with Fraser river water, ENSO-controlled variations in the isotopic composition of the precipitated water and $\delta^{18}\text{O}$ released from manure NO_3 (Wassenaar 1995). However, these parameters vary considerably in space and time and quantification of their contribution to the isotopic composition of the river water is extremely difficult.

This study demonstrated the broad applicability of the freshwater bivalve *M. falcata* for reconstructing past climates and ecosystem conditions in the LFV region of British Columbia. Further studies should focus on extending the chronology back in time by

using subfossil shell material. This could resolve the question whether the relationship between shell growth and precipitation has changed due to anthropogenic activity. It could help identify the precise effects that fertilizers, trace metals, pesticides, etc., exert on shell growth of *M. falcata*.

Acknowledgements Monthly precipitation and temperature data (University of Delaware dataset) as well as NINO1.2 and NINO3 indices were provided by the NOAA-CIRES Climate Diagnostics Center, Boulder, CO, USA, from their Web site at <http://www.cdc.noaa.gov/>. The KMNI Explorer (<http://www.climexp.knmi.nl>) was used for the preparation of spatial correlation charts. Wavelet transforms were computed with the ION script at <http://www.ion.researchsystems.com>. This study has been made possible by a German Research Foundation (DFG) grant (to BRS) within the framework of the Emmy Noether Program (SCHO 793/1).

References

- Ansell AD (1968) The rate of growth of the hard clam *Mercenaria mercenaria* (L) throughout the geographic range. *Journal du Conseil Perm Int pour l'Exploration de la Mer* 31:364–409
- Bauer G (1992) Variation in the life span and size of the freshwater pearl mussel. *J Anim Ecol* 61:425–436
- Berka C, Schreier H, Hall K (2001) Linking water quality with agricultural intensification in a rural watershed. *Water Air Soil Pollut* 127:389–401
- Bice KL, Arthur MA, Marinovich L Jr (1996) Late Paleocene Arctic Ocean shallow-marine temperatures from mollusk stable isotopes. *Paleoceanography* 11:241–249
- Boyle CA, Lavkulich L, Schreier H, Kiss E (1997) Changes in land cover and subsequent effects on Fraser Basin Ecosystems from 1823 to 1900. *Environ Manage* 21:185–196
- Briffa KR, Jones PD (1990) Basic chronology statistics and assessment. In: Cook ER, Kairiukstis LA (eds) *Methods of dendrochronology: applications in the environmental sciences*. Kluwer Academic Publishers, Dordrecht, pp 137–152
- Cameron EM, Hall GEM, Veizer J, Krouse HR (1995) Isotopic and elemental hydrogeochemistry of a major river system: Fraser River, British Columbia, Canada. *Chem Geol* 122:149–169
- Cane MA (2005) The evolution of El Niño, past and future. *Earth Planet Sci Lett* 230:227–240
- Chamberlain TK (1931) Annual growth of freshwater mussels. *Bull US Bur Fish* 46:713–739
- Cook ER, Kairiukstis LA (eds) (1990) *Methods of dendrochronology. Applications in the environmental sciences*. Kluwer Academic Publishers, Dordrecht, pp 1–394
- Cook ER, Buckley BM, D'Arrigo RD, Peterson MJ (2000) Warm-season temperatures since 1600 B.C. reconstructed from Tasmanian tree rings and their relationship to large-scale sea surface temperature anomalies. *Clim Dyn* 16:79–91
- Culp JM, Lowell RB (1999) Pulp mill effluent impacts on benthic communities and selected fish species in the Fraser River Basin. In: Gray C, Tuominen T (eds) *Health of the Fraser River aquatic ecosystem. A synthesis of research conducted under the Fraser River Action Plan, vol. 2*. DOE FRAP 1998-11. Environment Canada, pp 13–34
- Dunca E, Mutvei H (2001) Comparison of microgrowth pattern in *Margaritifera margaritifera* shells from south and north Sweden. *Am Malacol Bull* 16:239–250
- Dunca E, Mutvei H, Schöne BR (2005) Freshwater bivalves tell of past climates: but how clearly do shells from polluted rivers speak? *Palaeogeogr Palaeoclimatol Palaeoecol* 228:43–57
- Edmonds RL, Francis RC, Mantua NJ, Peterson DL (2003) Sources of climate variability in river ecosystems. In: Wissmar RC, Bisson PA (eds) *Strategies for restoring river ecosystems: sources of variability and uncertainty in natural and managed systems*. American Fisheries Society, Bethesda, pp 11–37
- Epstein S, Buchsbaum H, Lowenstam H, Urey C (1953) Revised carbonate-water isotopic temperature scale. *Geol Soc Am Bull* 64:1315–1326
- Feder HM, Pearson TH (1988) The benthic ecology of Loch Linnhe and Loch Eil, a sea-loch system on the west coast of Scotland: V. Biology of the dominant soft-bottom epifauna and their interaction with the infauna. *J Exp Mar Biol Ecol* 116:99–134
- Fluegel M, Sylvestre S, Tuominen T, Sekela M, Moyle G (2004) The effects of non-point source pollution in small urban and agricultural streams. Environment Canada Pacific & Yukon Region, Vancouver, EC/GB/04/77
- Fraser River Action Plan (1999) Lower Fraser Valley stream review. Volume 1: strategic review. Fisheries and Oceans Canada. Queens Printer, Vancouver, pp 1–442 (ISBN 0-662-26167-4)
- Gedalof Z, Peterson DL, Mantua NJ (2004) Columbia River flow and drought since 1750. *J Am Water Resour Ass* 40:1–14
- Giannico GR (2000) Habitat selection by juvenile coho salmon in response to food and woody debris manipulations in suburban and rural stream sections. *Can J Fish Aquat Sci* 57:1804–1813
- Goodwin DH, Flessa KW, Schöne BR, Dettman DL (2001) Cross-calibration of daily growth increments, stable isotope variation, and temperature in the Gulf of California bivalve mollusk *Chione cortezi*: implications for paleoenvironmental analysis. *Palaaios* 16:387–398
- Greater Vancouver Sewerage and Drainage District (GVS&DD) (1999) Assessment of current and future GVS&DD area watershed and catchment conditions. GVRD, Burnaby, pp 1–53
- Groisman PY, Easterling DR (1993) Variability and trends of total precipitation and snowfall over the United States and Canada. *J Clim* 7:184–205
- Grossman EL, Ku T-L (1986) Oxygen and carbon isotope fractionation in biogenic aragonite; temperature effects. *Chem Geol* 59:59–74
- Hall KJ, Anderson BC (1988) The toxicity and chemical composition of urban stormwater runoff. *Can J Civ Eng* 15:98–106
- Hall K, Schreier H (1996) Urbanization and agricultural intensification in the Lower Fraser Valley: impacts on water use and water quality. *GeoJournal* 40:135–146
- Hall TJ, Haley RK, LaFleur LE (1991) Effects of biologically treated bleached kraft mill effluent on cold water stream productivity in experimental stream channels. *Environ Toxicol Chem* 10:1051–1060
- Hansson S (1987) Effects of pulp and paper mill effluents on coastal fish communities in the Gulf of Bothnia, Baltic Sea. *Ambio* 16:344–348

- Hoerling MP, Kumar A (1977) Why do North American climate anomalies differ from one El Niño event to another? *Geophys Res Lett* 24:1059–1062
- Hsieh WW, Tang B (2001) Interannual variability of accumulated snow in the Columbia Basin, British Columbia. *Water Resour Res* 37:1753–1759
- IAEA (2001) GNIP Maps and Animations, International Atomic Energy Agency, Vienna. Accessible at <http://www.isohis.iaea.org>
- Jakob M, McKendry I, Lee R (2003) Long-term changes in rainfall intensities in Vancouver, British Columbia. *Can Water Resour J* 28:587–604
- Johnson PD, Brown KM (1998) Intraspecific life history variation in the threatened Louisiana pearlshell mussel, *Margaritifera hembeli*. *Freshw Biol* 40:1–13
- Jones DS, Arthur MA, Allard DJ (1989) Sclerochronological records of temperature and growth from shells of *Merccenaria mercenaria* from Narragansett Bay, Rhode Island. *Mar Biol* 102:225–234
- Kennish MJ, Lutz RA, Dobarro JA, Lowell LW (1994) In situ growth rates of the ocean quahog, *A. islandica* (Linnaeus, 1767), in the middle Atlantic Bight. *J Shellfish Res* 13:473–478
- Macdonald R, Hall K, Schreier H (1997) Water quality and stormwater contaminants in the Brunette River Watershed, British Columbia, 1994/95. Prepared for the Fraser River action plan and the Fraser Pollution Abatement Office (FPAO), by the Westwater Research Unit, Institute of Resources and Environment, University of British Columbia, pp 1–132
- Marsh R, Petrie B, Weidman CR, Dickson RR, Loder JW, Hannah CG, Frank K, Drinkwater K (1999) The 1882 tilefish kill—a cold event in shelf waters off the north-eastern United States? *Fish Oceanogr* 8:39–49
- McLeay DJ (1987) Aquatic toxicity of pulp and paper mill effluent: a review. Environmental Protection Series Report No. EPS 4/PF/1. Conservation and Protection, Environment Canada, Ottawa, pp 1–191
- Meko D, Stockton CW, Boggess WR (1995) The tree-ring record of severe sustained drought. *Water Resour Bull* 31:789–801
- Metcalfe-Smith JL, Green RH (1992) Ageing studies on three species of freshwater mussels from a metal-polluted watershed in Nova Scotia, Canada. *Can J Zool* 70:1284–1291
- Molnar P, Cane MA (2002) El Niño's tropical climate and teleconnections as a blueprint for pre-Ice Age climates. *Paleoceanography* 17:1–11
- Mook WG, Vogel JC (1968) Isotopic equilibrium between shells and their environment. *Science* 159:874–875
- Mutvei H, Westermarck T (2001) How environmental information can be obtained from Naiad shells. In: Bauer G, Wächtler K (eds) Ecology and evolution of the freshwater mussels Unionoidea. Ecological studies, vol. 145. Springer, Berlin Heidelberg New York, pp 367–379
- Oke T, Hay J (1998) The climate of Vancouver, 2nd edn. BC Geographical Series, No. 50, Vancouver, pp 1–84
- Rayner NA, Parker DE, Horton EB, Folland CK, Alexander LV, Rowell DP, Kent EC, Kaplan A (2003) Globally complete analyses of sea surface temperature, sea ice and night marine air temperature, 1871–2000. *J Geophys Res* 108:4407. DOI 10.1029/2002JD002670
- Rood KM, Hamilton RE (1995) Hydrological and water use for salmon streams in the Chilliwack/Lower Fraser Habitat Management Area, British Columbia. Canadian Manuscript Report Fisheries Aquatic Science 2288, pp 1–223
- Ropelewski CF, Halpert MS (1986) North American precipitation and temperature associated with the El Niño/Southern Oscillation (ENSO). *Mon Weather Rev* 114:2352–2362
- Ropelewski CF, Halpert MS (1987) Global and regional scale precipitation patterns associated with the El Niño/Southern Oscillation. *Mon Weather Rev* 115:1606–1626
- Ropelewski CF, Halpert MS (1989) Precipitation patterns associated with the high index phase of the Southern Oscillation. *J Clim* 2:268–284
- Schöne BR, Tanabe K, Dettman DL, Sato S (2003) Environmental controls on shell growth rates and $\delta^{18}\text{O}$ of the shallow-marine bivalve mollusk *Phacosoma japonicum* in Japan. *Mar Biol* 142:473–485
- Schöne BR, Dunca E, Mutvei H, Norlund U (2004) A 217-year record of summer air temperature reconstructed from freshwater pearl mussels (*M. margaritifera*, Sweden). *Quaternary Sci Rev* 23:1803–1816, 2057
- Schöne BR, Dunca E, Fiebig J, Pfeiffer M (2005) Mutvei's solution: an ideal agent for resolving microgrowth structures of biogenic carbonates. *Palaeogeogr Palaeoclimatol Palaeoecol* 228:149–166
- Schreier H, Hall KJ, Brown SJ, Wernick B, Berka C, Belzer W, Pettit K (1999) Agriculture: an important non-point source of pollution. In: Gray C, Tuominen T (eds) Health of the Fraser River aquatic ecosystem. A synthesis of research conducted under the Fraser River Action Plan, Volume 2. DOE FRAP 1998-11. Environment Canada, pp 83–100
- Shabbar A, Bonsal B, Khandekar M (1997) Canadian precipitation patterns associated with the Southern Oscillation. *J Clim* 10:3016–3027
- Stockton CW, Jacoby GC (1978) Long term surface-water supply and streamflow trends in the upper Colorado River basin. Lake Powell Research Project Report 18, pp 1–70
- Ting M, Wang H (1997) Summertime U.S. precipitation variability and its relation to Pacific sea surface temperature. *J Clim* 10:1853–1873
- Torrence C, Compo GP (1998) A practical guide to wavelet analysis. *Bull Am Meteor Soc* 79:61–78
- Toy KA (1998) Growth, reproduction and habitat preference of the freshwater mussel *Margaritifera margaritifera falcata* in western Washington. MSc thesis, University of Washington, pp 1–84
- Trenberth KE (1997) The definition of El Niño. *Bull Am Meteor Soc* 78:2771–2777
- Walker GT (1923) Correlation in seasonal variations of weather, VIII: a preliminary study of world weather. *Mem Ind Meteorol Dept* 24:75–131
- Wassenaar LI (1995) Evaluation of the origin and fate of nitrate in the Abbotsford Aquifer using the isotopes of ^{15}N and ^{18}O in NO_3^- . *Appl Geochem* 10:391–405
- Wefer G, Berger WH (1991) Isotope paleontology: growth and composition of extant calcareous species. *Mar Geol* 100:207–248
- Weidman CR, Jones GA, Lohmann K (1994) The long-lived mollusc *Arctica islandica*: a new paleoceanographic tool for the reconstruction of bottom temperatures for the continental shelves of the northern North Atlantic Ocean. *J Geophys Res—Oceans* 99:18305–18314
- Wernick BG, Cook KE, Schreier H (1998) Land use and streamwater nitrate-N dynamics in an urban-rural fringe watershed. *J Am Water Resour Assoc* 34:639–650
- Wigley TML, Briffa KR, Jones PD (1984) On the average value of correlated time series, with applications in dendroclimatology and hydrometeorology. *J Clim Appl Meteorol* 23:201–213